AMERICAN METEOROLOGICAL SOCIETY

EARLY ONLINE RELEASE

This is a preliminary PDF of the author-produced manuscript that has been peer-reviewed and accepted for publication. Since it is being posted so soon after acceptance, it has not yet been copyedited, formatted, or processed by AMS Publications. This preliminary version of the manuscript may be downloaded, distributed, and cited, but please be aware that there will be visual differences and possibly some content differences between this version and the final published version.

The DOI for this manuscript is doi: 10.1175/BAMS-D-13-00084.1

The final published version of this manuscript will replace the preliminary version at the above DOI once it is available.

The CHUVA Project – how does convection vary across Brazil?

Luiz A. T. Machado[1], Maria A. F. Silva Dias[2], Carlos Morales[2], Gilberto Fisch[3], Daniel Vila[1], Rachel Albrecht[1], Steven J. Goodman[4], Alan Calheiros[1], Thiago Biscaro[1], Christian Kummerow[5], Julia Cohen[6], David Fitzjarrald[7], Ernani Nascimento[8], Meiry Sakamoto[9], Christopher Cunningham[1], Jean-Pierre Chaboureau[10], Walter A. Petersen[11], David Adams[12], Luca Baldini[13], Carlos F. Angelis[1], Luiz F. Sapucci[1], Paola Salio[14], Henrique M. J. Barbosa[15], Eduardo Landulfo[16], Rodrigo F. Souza[17], Richard J. Blakeslee[18], Jeffrey Bailey[19] , Saulo Freitas[1], Wagner. F. A. Lima[1] and Ali Tokay[20]

1. Instituto Nacional de Pesquisas Espaciais (INPE). Centro de Previsão de Tempo e Estudos Climáticos (CPTEC), Brazil.
2. Universidade de São Paulo. Instituto de Astronomia, Geofísica e Ciências Atmosféricas, Brazil.
3. Departamento de Ciências e Tecnologia Espacial. Instituto de Aeronáutica e Espaço, Brazil
4. National Oceanic and Atmospheric Administration (NOAA/NESDIS/GSFC), USA
5. Colorado State University, Cooperative Institute for Research in the Atmosphere, USA
6. Universidade Federal do Pará, Instituto de Geociências, Brazil.
7. University at Albany, SUNY, Atmospheric Sciences Research Center, USA
8. Universidade Federal de Santa Maria, Departamento de Física, Brazil
9. Fundação Cearense de Meteorologia, Brazil
10. Laboratoired'Aérologie, University of Toulouse, France
11. NASA Wallops Flight Facility, USA
12. Universidad Nacional Autónoma de México, Centro de Ciencias de la Atmósfera, Mexico
13. CNR Istituto di Scienze dell'Atmosfera e del Clima, Italy
14. Universidade e Buenos Aires, Argentina
15. Universidade de São Paulo. Instituto de Física, Brazil
16. Instituto de Pesquisas Energéticas e Nucleares, Brazil.
17. Universidade do Estado do Amazonas, Brazil.
18. NASA Marshall Space Flight Center, Huntsville, Alabama USA
19. University of Alabama in Huntsville, Huntsville, Alabama USA
20. University of Maryland Baltimore County Baltimore, Maryland, USA

ABSTRACT

CHUVA, meaning "rain" in Portuguese, is the acronym for the *Cloud processes of tHe main precipitation systems in Brazil: A contribUtion to cloud resolVing modeling and to the GPM (GlobAl Precipitation Measurement)*. The CHUVA project has conducted five field campaigns; the sixth and last campaign will be held in Manaus in 2014. CHUVA's main scientific motivation is to contribute to the understanding of cloud processes, which represent one of the least understood components of the weather and climate system. The five CHUVA campaigns were designed to investigate specific tropical weather regimes. The first two experiments, namely, Alcantara and Fortaleza in northeast Brazil, focused on warm clouds. The third campaign, which was conducted in Belem, was dedicated to tropical squall lines that often form along the sea-breeze front. The fourth campaign was in the Vale do Paraiba of southeastern Brazil, which is a region with intense lightning activity. In addition to contributing to the understanding of cloud process evolution from storms to thunderstorms, this fourth campaign also provided a high fidelity total lightning proxy dataset for the NOAA GOES-R program. The fifth campaign was carried out in Santa Maria, southern Brazil, a region of intense hailstorms associated with frequent mesoscale convective complexes. This campaign employed a multi-model high resolution ensemble experiment. The data collected from contrasting precipitation regimes in tropical continental regions allow the various cloud processes in diverse environments to be compared. Some examples of these previous experiments are presented to illustrate the variability of convection across the tropics.

1

2

3

4   **Capsule**

5

6   *CHUVA reveals very diverse cloud processes in tropical continental regions and*

7   *contributes to improving satellite precipitation estimation, nowcasting, cloud resolving*

8   *models and the understanding of cloud electrification.*

9

1. Introduction

The CHUVA project began in 2010 and has conducted five field campaigns; the last experiment will be held in Manaus as part of *GoAmazon (Green Ocean Amazon),* in 2014 (see http://campaign.arm.gov/goamazon2014/ for a detailed description). CHUVA's main scientific motivation is to contribute to the understanding of cloud processes, which represent one of the least understood components of the climate system.

Brazil has an area of 8.5 million km^2 and lies primarily south of the Equator and within the tropics. Therefore, Brazil is ideally situated for studying tropical continental convection over a broad range of precipitation regimes within a single country. In the Northeast Brazil, a semi-arid region, the CHUVA project was designed to characterize warm clouds (Costa et al., 2000) and the organized convection influenced by the inter-tropical convergence zone and easterly waves (Kouadio al., 2012). Cotton (1982) defines warm clouds as clouds in which the ice phase does not play a substantial role in the precipitation process. In the Amazon, specifically in the Belem and Manaus regions, the main targeted precipitation regimes were tropical squall lines (Cohen et al., 1995); local convection, which is strongly forced by the diurnal cycle (Machado et al. 2002); and mesoscale convective systems (Rickenbach, 2004). In southern Brazil, at the boundary of the tropical and subtropical regions, CHUVA measured the convection associated with cold fronts (Garreaud, 2000), mesoscale convective complexes (Salio et al., 2007) and strongly electrified convection (Cecil and Blankenship, 2012). The field campaigns in each of these regions collected detailed observations of various

34   rainfall regimes over a tropical continental region to improve our understanding of

35   cloud processes. The campaigns focused on the following applications: satellite

36   precipitation estimation, cloud resolving models, nowcasting and cloud

37   electrification. CHUVA is contributing to the National Aeronautics and Space

38   Administration (NASA) - Japan Aerospace Exploration Agency (JAXA) Global

39   Precipitation Measurement (GPM), National Oceanic and Atmospheric

40   Administration (NOAA) Geostationary Operational Environmental Satellite R-series

41   (GOES-R) and GoAmazon Programs.

42   Schumacher and Houze (2003) demonstrated large seasonal and regional variability

43   in the stratiform rain fraction (the contribution of stratiform precipitation to the

44   total precipitation) over Brazil using the TRMM precipitation radar. Precipitation

45   estimation has been noticeably improved by the Tropical Rainfall Measuring

46   Mission (TRMM) and the development of new algorithms (Tapiador et al., 2012).

47   However, precipitation estimation over land using passive radiometers still has

48   several deficiencies. Specifically, precipitation is indirectly estimated (Berg et al.,

49   2006). Moreover, precipitation from warm clouds is largely underestimated,

50   especially when using microwave radiometers, and contributes (7.5% on average)

51   to the total rainfall in tropical coastal regions (Liu and Zipser, 2009). Over land,

52   microwave satellite precipitation estimates exploit the relationship between ice

53   aloft and rainfall at the surface. Because these clouds have no ice, the precipitation

54   estimates for warm cloud rainfall are inaccurate. For example, during November

55   2008, 283 mm of rainfall, mostly from orographic warm clouds, was measured by

56   rain gauge over twenty-four hours in southeastern Brazil. However, only very light

57   precipitation amounts (approximately 30 mm) were estimated using satellite data

58   (Silva Dias, 2009). Williams and Stanfill (2002) discuss the formation of warm cloud

59   rainfall in the context of cloud condensation nuclei and updrafts and contrast the

60   marine and continental environments.

61   The passive microwave rainfall sensors used by the GPM constellation to achieve

62   three-hour rainfall estimates have largely relied on ice scattering signals to convert

63   brightness temperature depressions into rainfall rates over continental regions.

64   The CHUVA field campaigns, in addition to their focus on the microphysical

65   properties of tropical clouds, have an important role in improving existing

66   algorithms for precipitation retrieval for the Global Precipitation Measurement

67   mission. Therefore, an important component of CHUVA was to provide a

68   homogeneous dataset to the community that supports GPM algorithm

69   development in both warm and cold phase clouds. As mentioned, warm rain clouds

70   are particularly challenging for the passive microwave remote sensing of

71   precipitation. CHUVA data will help address this issue.

72   The dataset collected in this project, combined with cloud modeling, is expected to

73   create a solid basis for the development of improved database on cloud process

74   over the continental tropics. This dataset contains hydrometeor classifications,

75   thermodynamics profiles, rainfall drop size distributions and several remote

76   sensing (both active and passive) cloud property measurements. Realistic

77   parameterizations of cloud processes are a prerequisite for reliable current and

78   future climate simulations. Meteorological models, at very high resolution,

79   explicitly describe cloud processes to a large degree; however, the cloud

80   microphysics and turbulent processes require parameterization. Morrison et al.

81   (2007) demonstrate the large sensitivity of high–resolution simulations to the

82   microphysical parameterizations. The CHUVA dataset, combining model, satellite,

83   radar, radiometer and other in-situ data, will provide an opportunity to validate

84   and improve cloud resolving models over various tropical continental regions.

85   GOES-R, the next generation of NOAA geostationary satellites, includes a new

86   capability for total lightning detection from the Geostationary Lightning Mapper

87   (GLM). The GLM will aid in forecasting severe storms, tornadic activity and will

88   address convective weather impacts on aviation safety and efficiency (Goodman et

89   al., 2013). The CHUVA measurements provide a high fidelity dataset for GLM

90   application development in continental tropical regions.

91   This study outlines the motivation for developing the CHUVA project and general

92   information on the measurement strategy and how to access the database and the

93   project webpage. Additionally, this study presents a specific description of each

94   field experiment, a discussion of the preparation for the final campaign, and a

95   summary of the main results and activities for project outreach.

96

97   **2. Motivation**

98

99   CHUVA's principal motivation is the description and understanding of the cloud

100   processes of the various precipitation regimes of Brazil. The expected results

101   include improved satellite precipitation estimates, especially from warm clouds;

102   cloud resolving model evaluation; development of nowcasting techniques for

103   intense thunderstorms; and an improved understanding of the cloud electrification

104   processes in the tropics/sub-tropics. The CHUVA project addresses the following

105   questions:

106   • *How can satellite estimates of warm cloud precipitation be improved?*

107   • *How can GPM satellite-based retrievals of rainfall over the continent be*

108   *improved?*

109   • *What are the typical cloud processes that occur in the main precipitation*

110   *regimes of Brazil?*

111   • *What are the major surface and boundary layer processes relevant to the*

112   *formation and maintenance of clouds?*

113   • *What are the primary processes in the evolution from shallow to deep*

114   *convection and how do cloud microphysical and electrification processes*

115   *evolve during this transition and cloud life cycle?*

116   • *How can the representation of clouds and accuracy be improved in cloud*

117   *resolving models, especially for* intense thunderstorms*?*

118   • *How can all of the acquired knowledge be utilized to improve nowcasting*

119   *and forecasting in tropical regions?*

120

121 To answer these questions, the CHUVA Project focused on collecting data that

122 describes the multi-dimensional structure of clouds in different precipitation

123 regimes. These data include: a) The selected cloud properties from XPOL and MRR

124 data; b) satellite and radar precipitation fields, cloud type classification and cloud

125 and rain cell life cycles; c) the electric fields and lightning associated with clouds

126 from the lightning network and field mills (an electro-mechanical device which

127 measures the strength of the electrostatic field at the surface), which are essential

128 for describing thunderstorm electrification processes; and d) mesoscale

129 atmospheric conditions and surface fluxes from rawinsondes and from towers to

130   assess the atmospheric dynamical and thermodynamic properties. These data are

131   combined with a cloud resolving model (the Brazilian version of the Regional

132   Atmospheric Modeling System - BRAMS) to describe the typical cloud processes of

133   the various precipitation regimes. As proposed by Negri et al. (2013), comparing

134   satellite and/or radar measurements with virtual images simulated by radiative

135   transfer and cloud resolving model outputs can validate the model and create a

136   microphysical database.

137   These datasets are specifically used to (1) test different methodologies for

138   estimating warm cloud precipitation, (2) evaluate the possible relationships

139   between integrated ice content, electrification and precipitation as functions of the

140   cloud life stage, (3) employ different satellite rainfall algorithms and assess the

141   associated regional errors, (4) describe the temporal evolution of the electrical

142   field during thunderstorm development in conjunction with the radar polarimetric

143   variables, (5) investigate the column-integrated atmospheric water vapor during

144   periods preceding intense thunderstorms and (6) analyze the capability of cloud

145   resolving models to describe the microphysical properties and the effect of the

146   turbulence parameterization on cloud organization.

147

148   **3. Experimental Design**

149

150   **a) Sites and Measurement Strategies**

151

152   CHUVA consists of six field campaigns, five of which have already taken place. The

153   sixth will be carried out in 2014 in Manaus as part of the GoAmazon initiative

154   (http://campaign.arm.gov/goamazon2014/). Figure 1 (left panel) shows the

155   experimental sites of the CHUVA projects and illustrates the main precipitation

156   regime expected in each region. Figure 1 (right panel) shows a schematic

157   representation of the measurement strategy employed in the CHUVA campaigns. A

158   primary instrument used for CHUVA is a mobile X-band dual polarization radar (X-

159   Pol). Schneebeli et al. (2012a and 2012b) give a detailed description of the radar,

160   operation and data processing. The radar scan strategy consists of a volume scan

161   with 10 to 14 elevations (depending on the main type of clouds targeted) and at

162   least one Range-Height Indicator (RHI) scan along the direction of the main

163   instrumentation site. The RHI is performed with an antenna rotation rate of nine

164   degrees per second, a high angular resolution (every 0.50°) and a high sampling

165   frequency (obtained using 150 samples per ray) to ensure a high vertical resolution

166   and data accuracy. The entire procedure (strategy) also includes a differential

167   reflectivity (Zdr) offset check using a vertical measurement along the column above

168   the radar. Figure 1 presents a typical description of the measurement strategy. The

169   distance between the radar site and the main site is approximately 20 km; the

170   main site is equipped with the following basic instruments (see Table I for a

171   detailed description): impact (Joss-Valdwogel) and laser (OTT Parsivel and Thies)

172   disdrometers; rain gauges (tipping bucket employed in a dual gauge configuration

173   at the main site); a microwave radiometer (MP3000A with 35 channels) ranging

174   from 22.00 to 30.00 GHz (21 channels), range associated with water vapor

175   emissions, and from 51.00 to 59.00 GHz (14 channels), range associated with

176   molecular oxygen emissions (Ware et al., 2003). Additionally, the main site

177   instrumentation includes one vertically pointing K-Band (24.1 GHz) micro rain radar

178   (MRR) (see Peter et al. (2005) for a detailed description), a Raman lidar at 532/604

179   nm, a GPS dual-frequency receiver to retrieve the column-integrated atmospheric

180   water (Sapucci et al., 2007), a field mill and a surface weather station to measure

181   surface latent and sensible heat fluxes, soil moisture and temperature. In addition

182   to the main site, two to four other sites instrumented with disdrometers, rain

183   gauges, a GPS receiver and field mills (variable number) were installed at various

184   distances from the radar. Rawinsondes were routinely released (at least twice a

185   day). During specific intensive observation periods (IOPs), a triangle of rawinsondes

186   in a nearly equilateral arrangement was launched 4 times a day (00:00, 06:00,

187   12:00 and 18:00 UTC).

188

189   **b) Data Access and the CHUVA Web Page**

190

191   The CHUVA website – http://chuvaproject.cptec.inpe.br – is the primary access to

192   the CHUVA information and data. For each campaign, a specific webpage was

193   developed (Figure 2). These web pages contain a wide variety of information

194   including the daily weather report, instrument strategy, instrument locations, quick

195   looks of the main events, data reports, cloud pictures and the SOS-CHUVA (Severe

196   storm Observation System), a geographical information system that utilizes data

197   from the CHUVA project and allows retrospective access to the radar, satellite and

198   model images, when available. The use of SOS-CHUVA for nowcasting will be

199   discussed in more detail in section 5. The CHUVA dataset has been pre-processed

200   and is available through the CHUVA website. Data can be accessed at different

201   levels. For example, level 0 data from the X-band radar are raw data in ASCII and

202   universal format (UF), level 1 data consist of the attenuation-corrected (Zh and Zdr)

203   data in ASCII and UF (see Testud et al., 2000, for a detailed description of the

204   attenuation correction), and level 2 data consist of the corrected reflectivity

205   constant altitude plan position indicators (CAPPIs) at various altitude levels.

206   Additional corrections, such as the correction for bias due to a wet radome and the

207   ZDR offset adjustment, are not applied in this dataset. However, instructions and

208   tables are accessible to the users for their own applications. Data for each

209   instrument comes with a "readme" file with information about the data and how

210   to manipulate the files. All raw data and several processed data (level 2) are

211   publicly available through the CHUVA website.

212   In addition, the CHUVA datasets for each campaign include the available

213   operational S-band radar data covering the field campaign region (see Table I for a

214   description of additional instrumentation), the GOES and Meteosat geostationary

215   satellite images (infrared channels) and all overpasses of the operational

216   environmental low-orbiting satellites carrying passive microwave sensors (channels

217   similar to TRMM-TMI).

218

219   **4. Field Campaigns**

220

221   **a) Alcantara**

222

223   Alcantara was the first CHUVA campaign from March 1-25, 2010. In addition to the

224   array of CHUVA instruments, the Alcantara experiment employed the Advanced

225   Microwave Radiometer for Rain Identification (ADMIRARI) (see Battaglia et al.

226   (2011) for a detailed description). The ADMIRARI measurements consist of passive

227   radiances collected at vertical and horizontal polarization at frequencies of 10.7,

228   21.0 and 36.5 GHz, and one co-staring active radar (MRR). The ADMIRARI were

229   pointed at a fixed 30° elevation angle oriented along a radial directed toward the X-

230   Pol radar located at a range of 7.65 km. Along the line between the X-Pol radar and

231   the ADMIRARI, two additional sites measured rainfall and drop size distributions.

232   Three distinct weather conditions were observed during the campaign. During the

233   first period (1 to 9 March) the convection was suppressed with only scattered

234   clouds and sparse rainfall. The second period (10 to 16 March) was characterized

235   by the beginning of the wet season with isolated local convection and dominant

236   warm cloud processes. The last period (16 to 25 March) experienced intense

237   convection with warm and deep (cold cloud/ice phase) convection, with

238   precipitation rates as high as 150 mm h^{-1}, the 99th percentile corresponds to 137

239   mm h^{-1} (the rain rate information described in this study was computed using rain

240   gauge tipping buckets integrated over one-minute intervals). The warm rainfall

241   events in Alcantara were associated with the highest concentration of large drops

242   (larger than 4 mm). Battaglia et al. (2011) describes two precipitation events during

243   the campaign in which the 21.0 and 36.5 GHz channels and the MRR were

244   repeatedly saturated with heavy rain. In one event, the 10 GHz signal was

245   saturated, which was the first time the ADMIRARI operation ever observed

246   saturation on this channel (this was the third ADMIRARI campaign). TRMM co-

247   located 2A25 version-7 near-surface precipitation radar was compared against the

248   precipitation measured during the CHUVA campaign by rain gauge. Alcantara

249   precipitation estimation from TRMM is underestimated by more than 50%. Of all

250   the campaigns to date, Alcantara has the highest average rainfall rate from warm

251   clouds (7.2 mm h^{-1}), one of the largest vertically integrated water vapor values and

252   high cloud water contents for non-precipitating clouds (0.34 mm), only slightly

253   smaller than observed in Belem. Alcantara also has the highest CAPE; the 99th

254   percentile corresponds to 1950 J Kg^{-1}.

255

256   **b) Fortaleza**

257

258   The data collection period spanned April 3-28, 2011, during the rainy season. The

259   main site was installed in the yard of the Civil Defense Organization (the

260   organization responsible for responding to natural disasters) in Fortaleza. A

261   partnership with Fundação Cearense de Meteorologia e Recursos Hídricos

262   (FUNCEME) was established for monitoring intense thunderstorms. The X-Pol radar

263   was installed in the city of Osorio, 20.5 km from the main CHUVA site. Additionally,

264   three more sites with disdrometers, rain gauges and GPS receivers were installed

265   around Fortaleza, and the most distant was 32.6 km from the radar. Given that the

266   focus of this campaign was warm cloud processes and deep convection associated

267   with the inter-tropical convergence zone (ITCZ), a volume scan strategy was

268   implemented with thirteen elevations focusing on both the lower and upper

269   troposphere (i.e., warm and deep cloud types). As already mentioned, the strategy

270   for all campaigns included a Zdr offset check and RHIs scans. For Fortaleza, two

271   RHIs scans were performed: one over the main site and another at 180 degrees,

272   perpendicular to the coast, where most systems propagate into the continent.

273   Three complete scans (volume scan, RHIs and vertically pointing) were run in 20-

274   minute cycles and a zero check (background noise estimation) was performed once

275   per hour.

276   Rawinsondes were launched in Fortaleza every six hours. However, in the time

277   interval of April 8-17, two additional sites located 135 km away in the cities of

278   Quixeramobim and Mossoró were added, and these began to launch rawinsondes

279   concurrently. This nearly equilateral triangular sounding array was designed to

280   cover mesoscale systems penetrating the continent. During this period, multiple

281   organized convective systems crossed the array in succession.

282   The maximum rainfall intensity recorded during the campaign was 152 mm h^{-1},

283   with the drop size distributions (DSDs) revealing a large population of large (> 4

284   mm) raindrops. Fortaleza had the largest average vertically integrated water vapor

285   (56.1 mm) and the highest melting level (4.7 km). These characteristics suggest

286   that the rainfall events in Fortaleza appear to have a very important warm process

287   when producing rain drops. Additionally, the stratiform rainfall in Fortaleza

288   exhibited the highest and least prominent bright-band (BB) peak intensity

289   (Calheiros and Machado, 2013). Fortaleza had the second highest CAPE; the 99th

290   percentile corresponds to 1840 J Kg^{-1}.

291

292   **c) Belem**

293

294   The Belem campaigns was performed during the period June 1-30, 2011, toward

295   the end of the wet season and during the period of maximum squall line frequency

296   (see Garstang et al. (1994) and Cohen et al. (1996) for a detailed description on

297   Amazonian squall lines). Negri et al. (2000) used a satellite-derived gauge-adjusted

298 precipitation climatology from microwave measurements, i.e., the Goddard

299 Profiling algorithm. They found a persistent local rainfall maximum at 1800 LST,

300 which moved inland at 21:00 LST, due to interactions between sea-breeze and

301 squall line formation and propagation into the Amazon along the northern coast of

302 Brazil.

303 The X-Pol radar was installed on the roof of the Meteorology Department of the

304 Federal University of Pará along the Guama River, a tributary of the Amazonas

305 River. Two main sites were set up, one in Outeiro and another in Benevides, 23.0

306 and 27.7 km from the radar, respectively. In general, rawinsondes were launched

307 twice daily in Belem, with the exception of an intensive observation period from

308 June 18-26, during which four rawinsondes were launched daily in the cities of

309 Tomé Açu and São Miguel, approximately 120 km apart. The radar volume scan

310 strategy was similar to that used in the previous experiments. Additionally, within

311 the ten-minute scan period strategy, ten more RHIs were performed (separated by

312 1.5 degrees) perpendicular to the Amazonas River covering the rawinsondes

313 triangle network. In addition to the typical CHUVA instrumentation, a mesoscale

314 GPS meteorological network was established (Adams et al. 2011) with fifteen

315 stations in close proximity (a 5 km to 10 km separation distance within Belem and a

316 40 km distance outside of Belem). This GPS network provided very high spatial and

317 temporal resolution for the column-integrated atmospheric water vapor and its

318 variability. Additionally, three field mill sensors were installed at Belem and the

319 main sites. Finally, controlled meteorological (CMET) balloons (Voss et al. 2005)

320 were launched from Tomé-Açu, Pará. These balloons are altitude controlled via

321 satellite, and the winds were determined using GPS tracking and a package carrying

322   temperature and moisture sensors. Two CMETs were launched twelve hours apart.

323   The CMET measurements, i.e., temperature and relative humidity, show the same

324   boundary layer structure as the Tomé-Açu rawinsondes. Each CMET was recovered.

325   The CMETs landed in the Tocantins River after six hours of flight. During the flights,

326   a mesoscale convective system to the south led to a strong directional wind shear

327   in the lower layers. Preliminary numerical studies using the BRAMS model

328   employing back trajectory are consistent with a southerly flow in response to a

329   depression associated with the interaction of a mesoscale convective system and a

330   developing sea breeze, which also promoted a southerly flow.

331   Several squall lines formed along the coast and sea breeze front, propagating

332   inland over the Amazonian rainforest, as described earlier by Cohen et al. (1995).

333   However, several of the observed squall lines were not initiated along the coast but

334   along the boundary of the rain forest and the semi-arid region to the east of Belem.

335   These squall lines propagated almost parallel to the coast. Another interesting

336   feature was the multi-scale nature of these large squall lines. Embedded in the

337   large cloud deck, successively smaller scale propagating rainfall cell lines were

338   detected by the radar. Figure 3 displays one example of the consecutive RHI scans

339   through the squall line on June 7, 2011. A typical vertical cross-section of the

340   evolving squall line is apparent; initially shallow warm clouds develop, followed by

341   rapidly deepening clouds up to 14 km. Following the convective region, the

342   stratiform sector evolved with a clear bright-band and a cloud top approximately

343   13 km at 22:00 UTC. During the dissipation phase (cloud collapse), the cloud top

344   height decreases and the bright-band region intensifies. The bright-band signature

345   is the result of complex microphysical processes that occur when snowflakes melt

346 in stratiform precipitation (Fabry and Zawadsky, 1995). More than twenty rain

347 events crossed the experimental region; the rain rate at the 99th percentile was

348 122 mm h^{-1}. The CAPE was also very high. However, the CAPE was less than at

349 Alcantara and Fortaleza; the 99th percentile corresponds to 1380 J Kg^{-1}.

350

351 **d) Vale do Paraíba**

352

353 The Vale do Paraíba campaign had the longest duration, with an IOP from

354 November 1 to December 22, 2011, followed by a second period with less intensive

355 measurements continuing through March 31, 2012. The instrumentation was

356 installed along a line perpendicular to the coast. The radar was 90 km inland from

357 the ocean at an elevation of 650 m. The main site was installed 11 km from the X-

358 Pol radar, and a succession of sites (spaced by approximately 20 km) was installed

359 along a line perpendicular to the ocean. These sites had at least one GPS IPW

360 (Integrated Precipitable Water) station, one disdrometer and multiple rain gauges.

361 Additionally, five field mills, spaced 1 km apart, formed a very high spatial

362 resolution array close to the radar. The radar strategy was designed to run for six

363 minutes.

364 During November and the first week of December, the region had an anomalous

365 southeasterly flow, decreasing the air temperature and increasing convective

366 inhibition. From the second week of December to March, several intense

367 thunderstorms and some severe weather events were reported in the region.

368 The primary objective of this campaign was to study storm electrification. As such,

369 comprehensive ground-based measurements of total lightning activity were

370   collected to improve our understanding and knowledge of thunderstorm initiation

371   and behavior and also develop more advanced nowcasting tools that combine

372   radar, lightning, satellite and numerical weather prediction (Goodman et al., 2012).

373   The second objective was to conduct cross-network inter-comparisons and

374   capability assessments of operational and research ground-based regional 2-D and

375   3-D total lightning mapping networks that might be useful for merging with or

376   validating the space-based lightning measurements becoming available late this

377   decade. This specific component of the field experiment included a very successful

378   collaboration among Brazilian, US, and European organizations (from universities

379   and industry). The participating lightning location systems (LLSs) were STARNET

380   (Sferics Timing And Ranging NETwork), RINDAT (Rede Integrada Nacional de

381   Detecção de Descargas Atmosféricas), WWLLN (World Wide Lightning Location

382   Network), ATDnet (Arrival Time Difference network), Vaisala GLD360 (Global

383   Lightning Dataset) and TLS200 (Total Lightning Sensor), BrasilDAT (Sistema

384   Brasileiro de Detecção de Descargas Atmosféricas), LINET (Lightning Network), and

385   LMA (Lightning Mapping Array). The last four networks were deployed along a

386   short baseline for total (intracloud and cloud-to-ground) lightning detection in

387   support of the development of proxy datasets and validation protocols in

388   preparation for the next generation of operational weather satellites (Goodman et

389   al., 2013) and the Meteosat Third Generation Lightning Imager in 2018 (Holler et al.,

390   2013). The lightning measurements provided by these LLSs were made

391   concurrently with overpasses of the TRMM Lightning Imaging Sensor (LIS) and the

392   SEVIRI (Spinning Enhanced Visible and Infrared Imager) on the Meteosat Second

393   Generation satellite. A 10-station Lightning Mapping Array network, expanded to

394   twelve stations in early December and then providing near-real time data, was

395   deployed over the eastern region of the Vale do Paraiba in the vicinity of São Paulo

396   to be one of the references for total lightning measurements. The distance

397   between the LMA stations was 15-30 km, and the network "diameter" was

398   approximately 60 km. Bailey et al., (2011) discuss a similar LMA configuration that

399   provides accurate 3-D lightning mapping and good detection efficiency as far as

400   150 km from the network center. This specific network installed in CHUVA has no

401   information about the specific efficiency detection; this information will be

402   available only after the cross-network inter-comparisons.

403   The combined lightning, satellite and radar data provide the most comprehensive

404   dataset to date. The dataset prepares users for the next generation of

405   geostationary satellite imagery and lightning mappers using SEVERI and LIS

406   measurements. Figure 4 presents an example of the characteristic lightning data

407   collected during one overpass of the TRMM satellite. The LMA, as well as the LIS,

408   were able to detect and locate lightning from various sub-components of individual

409   flashes.

410   Additionally, nowcasting applications were tested based on detailed information of

411   intense thunderstorms that produced hail, damaging winds and flooding over the

412   metropolitan area of São Paulo and Vale do Paraiba. Figure 5 provides an example

413   of a severe weather event that produced very large hail (up to 20 mm) and flooding

414   in the region. A rapid increase in lightning source numbers, known as the

415   "lightning-jump", firstly discussed by William et al., (1999), is associated with

416   severe weather, occurred in advance of the hail event. Figure 5A shows the 15-

417   minute accumulated LMA source density (number of sources in a 1x1 km^2 grid

during a 15-minute period) plotted in latitude-longitude, latitude-height and longitude-height projections and the observed signature of the lightning-jump. This cell was initiated southwest of Sao Paulo and traveled through Sao Paulo and Guarulhos cities with reflectivities greater than 40 dBZ from 1700 to 1830 UTC, reaching values greater than 65 dBZ at 1745 UTC when hail was reported in downtown Sao Paulo. Moreover, 15 minutes later, hail and flooding were reported in Guarulhos, which corresponds with the maximum observed LMA sources (Figure 5B). The electrical structure of this cell exhibited two well-developed charge centers with maximum activity near 1800UTC. This lighting source maximum (lightning-jump) and has been associated with severe weather, including tornados (Schultz et al., 2009). The lightning activity had two major source regions at approximately 7 km and 10 km. These thunderstorms extended to a height of 18 km. Cloud electrification is tightly controlled by updrafts and precipitation formation. Therefore, monitoring lightning activity inside a cloud can lead to severe weather warnings detected by a lightning-jump signature.

The LMA mapped the convective cells in near real-time. The most recent 10 minutes of the LMA lightning data were uploaded to the CHUVA nowcasting website (SOS) every 5 minutes. This site provides civil defense, management organizations, electrical power companies and the public with information on real-time convection and lightning threat.

During the Vale do Paraiba campaign, several intense thunderstorms and some severe weather events were recorded, including a downburst, causing destruction of many trees, and many cases of hailstorms. The rain rate at the 99th percentile at the main site was 137 mm h^{-1}. Warm clouds during the Vale do Paraiba campaign

442   had a lower frequency and average rain rate than the others CHUVA tropical sites.

443   Moreover, non-precipitating clouds exhibited a small average measured value

444   (0.13 mm) and the largest difference with the adiabatic calculation. One possible

445   reason for this finding is the dry entrainment effect that reduces the liquid water

446   content below the estimated adiabatic value. The CAPE value at vale do Paraiba

447   was nearly identical to the observations in Belem; the 99th percentile corresponds

448   to 1260 J Kg^{-1}. The Vale do Paraiba and Santa Maria locations had a very small

449   average integrated water vapor amount (27 and 29 mm, respectively) compared

450   with the sites located closer to the equator.

451

452   **e) Santa Maria**

453

454   The Santa Maria campaign, named CHUVA SUL, took place from November 5 to

455   December 12, 2012. Zipser et al. (2006) report that very intense thunderstorms are

456   observed in this region and mesoscale convective systems organized by the

457   penetration of cold fronts are common. Liu et al. (2010) used a 10-year satellite

458   database from TRMM to show that most precipitation in this region (more than

459   2000 mm/year) comes from thunderstorms. During the campaign, the rain rate at

460   the 99th percentile was 106 mm h^{-1}. Six mesoscale convective systems crossed the

461   region during the campaign, with intense activity confined primarily to Argentina

462   and Uruguay. On 1 December, a convective event brought down trees near the

463   main site and was considered the most intense storm crossing the sites.

464   Unfortunately, the X-band radar suffered a voltaic arc and could not be repaired in

465   time for the campaign. However, two S-band radars operated by the Brazilian Air

466   Force, one in Santiago and another in Cambuçu, 100 km and 180 km from the main

467   site, respectively, made measurements during this event. These radars ran a

468   volume scan strategy, employing 15 elevations every ten minutes. All of the CHUVA

469   instruments were installed similar to the other campaigns using rainfall

470   measurement sites, a GPS mesoscale network and a field mill network. Additional

471   instrumentation included surface weather stations in a mesoscale network

472   composed of six stations spaced 20 km apart. The rawinsondes were launched

473   twice a day. During the occurrence of organized systems, soundings were also

474   launched every six hours in Santiago and Cruz Alta, approximately 120 km apart.

475   The Santa Maria campaign showed the lowest value for CAPE; the 99th percentile

476   corresponds to only 400 J Kg^{-1}, larger values were only observed closed to the six

477   main events. A unique activity in CHUVA SUL was the use of the High Resolution

478   Limited Area Model Ensemble (HRLAMENS). The HRLAMENS effort was developed

479   under mutual collaboration between CHUVA and the LPB-RDP (La Plata Basin -

480   Research and Development Project, which focuses on high impact weather), which

481   aimed to furnish additional information on the total amounts and locations of

482   precipitation and their uncertainties. The HRLAMENS was composed of five models

483   (two versions of the BRAMS model and three versions of the Weather Research

484   and Forecasting (WRF) model), which were integrated using the Centro de Previsão

485   de Tempo e Estudos Climáticos (CPTEC) supercomputing facilities. Moreover, four

486   others model configurations were ran in others Institutions in Brazil and Argentina.

487   This core set of models was designed to be driven by selected global ensemble

488   prediction system members from CPTEC and the National Centers for

489   Environmental Prediction. The simulations were homogeneous in domain size and

490   horizontal and vertical resolution (2 km grid spacing and 41 levels). Partner

491   institutions in the project assisted with the multi-model composition in their

492   respective model (WRF running in University of Buenos Aires, WRF running at

493   University of Santa Maria and MESO-NH from the Laboratoire d'Aerologie (France)).

494   The results are still being evaluated. Nevertheless, preliminary conclusions indicate,

495   as expected, sensitivity to the lateral boundary conditions and model

496   characteristics. The ultimate objective is to find an optimal balance among

497   ensemble members that would improve the current state of rainfall predictions for

498   the region.

499

500   **f) GoAmazon - Manaus.**

501

502   The GoAmazon experiment seeks to understand the interaction of aerosol and

503   cloud life cycles. The GoAmazon experiment will be performed in Manaus, a

504   megacity of almost 1.8 million people in the central Amazon. Two intensive

505   operating periods (IOP) are being prepared for 2014, one in February-March,

506   during the wet season, and another in September-October, at the end of the dry

507   season. The GoAmazon experiment consists of several combined efforts, including

508   the deployment of the ARM mobile facility (Cadeddu et al., 2013), the Grumman

509   Gulfstream 159 (G-1) aircraft (from the Pacific Northwest National Laboratory) to

510   collect chemistry and microphysical properties, ACRIDICON (Aerosol, Cloud,

511   Precipitation, and Radiation Interactions and Dynamics of Convective Cloud

512   Systems) with the High Altitude and Long Range Research Aircraft (HALO), which is

513   the new research aircraft of the German Science Community (Gulfstream G-550)

514   and the CHUVA project. The CHUVA campaign will employ an X-Pol measurement

515   strategy, which provides volume scans and several RHIs over the sites in

516   coordination with the ARM cloud radar. It is important to note that the GPM core

517   observatory will be launched during the first IOP. Hence, there will be an

518   opportunity to combine data from the TRMM and GPM core satellites with those

519   collected during GoAmazon to study cloud and precipitation processes over one of

520   the rainiest continental regions of the planet.

521

522   **5. CHUVA Outreach**

523

524   **a) The CHUVA-SOS Nowcasting system**

525

526   The SOS-CHUVA is a web-based geographic information system combining

527   observations from radar, lightning networks, satellite images, numerical models

528   and nowcasting procedures. This is a useful tool to interpret, summarize and

529   integrate the environmental information and display and send warnings for

530   emergency management groups. In addition, SOS_CHUVA is an open access system

531   serving the population through real time information, thereby reducing citizen

532   vulnerability. By taking advantage of the instrumentation employed in each

533   campaign, a nowcasting pilot project is set up for each region, which addresses

534   specific vulnerabilities and needs. The SOS-CHUVA provides high resolution radar,

535   satellite and lightning data nearly in real time. It also provides the results from

536   several nowcasting applications, including the radar forecast for the next ten

537   minutes (based on Fortracc, Vila et al., 2007, and the Rainbow data processing

538 system software) and the lightning probability (Machado et al., 2009), among

539 several other functions, such as the total integrated precipitation for each

540 neighborhood. For the regions outside of the radar coverage, the system provides

541 information based on the hydroestimator and the Fortracc nowcasting cloud

542 systems for the following two hours using geostationary satellite data. The system

543 also provides forecast data from the BRAMS cloud resolving model at a resolution

544 of a few kilometers. The SOS-CHUVA in each campaign was developed in

545 partnership with the local civil defense and fire departments.

546

547 **b) Training and Education and Workshop**

548

549 Outreach activities are an important component of the CHUVA project. For

550 example, training lectures were presented to local students during each campaign

551 via a one-week course that covered themes of nowcasting, cloud resolving models,

552 polarimetric radar, satellite data usage, lidar, GPS and cloud microphysics. The

553 lectures were offered to graduate and undergraduate students in environmental

554 sciences; more than 100 students attended each campaign course. The programs

555 and details of each course are available from the specific webpage of the campaign.

556 Finally, an international workshop was organized in May 2013 in São Paulo. Access

557 to the abstracts and the presentations is available at the following URL:

558 http://chuvaproject.cptec.inpe.br/portal/workshop/index.html.

559

560 **6. Discussion.**

561

562   The use of similar instruments across campaigns in the various precipitation

563   regimes makes it possible to study the regional contrasts and correspondences.

564   Figure 6 illustrates examples of similarities and differences among the various

565   precipitation regimes. Figure 6A shows the DSD adjustment to the gamma function

566   (using the momentum method described by Tokay and Short, 1996) in the three-

567   dimensional space of the gamma parameters: the intercept (N_0) in the x axis, the

568   shape (m) in the y axis and the width (Λ) in the z axis, using the same procedure

569   employed by Cecchini et al. (2013). In this three-dimensional space (a logarithmic

570   option is applied to N_0 to adjust the data to the same range), the DSD gamma

571   parameters are represented for the Vale do Paraiba, Belem and Santa Maria

572   campaigns. Each point in this diagram corresponds to a specific DSD. We note the

573   regional differences in the frequency of occurrence over the gamma parameter´s

574   spatial domains. However, it is very interesting to see that all points, regardless of

575   the regime, are nearly over the same adjusted surface. Therefore, we can

576   parameterize the Gamma distribution using only two independent parameters. The

577   raindrop size distribution characteristics observed by surface based disdrometers

578   can distinguish different precipitation systems. Tokay et al. (2002) demonstrated

579   the presence of more large drops and small concentration in easterly regime than

580   in the westerly regime in the southwestern Amazon basin. In their study, DSD

581   differences were also observed between the monsoon and break regimes in

582   Northwest Australia. The DSD features from CHUVA will be analyzed in detail after

583   the completion of the GoAmazon project.

584   Another example of regional contrasts/similarities is presented in Figure 6B using

585   the warm cloud-ice cloud index (WII). The WII is defined as the ratio of the

586   difference between the cloud thickness of the cloud layer below and above the

587   freezing level and the total cloud thickness (see Figure 6b for a schematic view and

588   the associated equation). The WII was computed using the vertical profile of

589   reflectivity (VPR) by employing data from the X-Pol RHI scanning mode and the co-

590   located rawinsondes (+-3 hour interval) over the main site. Only continuous cloud

591   layers were considered in this analysis; multi-layer clouds were discarded. A

592   continuous layer cloud was defined as having a continuous layer with values larger

593   than 0 dBZ in the warm sector and -10 dBZ in the layer above the 0°C isotherm.

594   Different thresholds were used because ice has a smaller refractive index than

595   liquid water. All rain events (rain rate greater than 0.1 mm h^{-1}) from non-

596   multilayers clouds and when rawinsonde data were available were computed in

597   the WII analysis. The thickness of the layer under the melting layer (L1) was defined

598   as the layer between the lifting condensation level (LCL) and the melting level

599   (both obtained from rawinsondes). The LCL is used to avoid possible rain layers

600   detected by the radar below the cloud base. The parameter L2, characterizing the

601   layer above the melting layer, is defined as the thickness of the layer between the

602   melting level and the last level of the continuous layer of reflectivities larger than -

603   10 dBZ. L2 roughly represent the cloud layer above 0°C isotherm, because radar

604   does not detect the cloud boundaries. The WII ranges from 1 (a pure warm cloud)

605   to -1 (clouds associated only with ice and/or supercooled water). Figure 6b

606   presents the rainfall cumulative frequency for each WII value. The cumulative

607   rainfall is obtained from a disdrometer located at the main site along the RHI

608   azimuth direction employed to build the VPR. The population for each site (rainfall

609   cases at the main site were associated with a single layer cloud that occurred

610   within the six-hour interval centered on the rawinsonde launch time) is variable,

611   ranging from 116 in Alcantara to 1500 Vale do Paraiba, depending on the number

612   of rainy days, the frequency of multilayer clouds and the duration of the campaign.

613   The cumulative rainfall, for each site, is presented as function of the WII values in

614   Fig. 6b to give an information about the specific cloud population of WII values in

615   the total rainfall. Two different behaviors can be observed in Fig. 6b.The first

616   behavior corresponds to negative WII values, responsible for approximately 70%-

617   75% of the total precipitation amount. Vale do Paraiba and Belem exhibit deep

618   clouds with a layer L2 above the melting level that is nearly three times larger (a

619   WII value of approximately -0.5) than the warm layer L1; for Fortaleza and

620   Alcantara, this layer is only 1.5 times larger than the warm layer (a WII around -0.3).

621   The second behavior, accounting for the remaining 30%-25% of precipitation, is

622   nearly linearly distributed for the positive values of the WII, expect for Vale do

623   Paraiba. These clouds are characterized by rain processes that are primarily below

624   the melting layer. Alcantara, Belem and Fortaleza present a very similar behavior;

625   approximately 25% of the precipitation is from clouds with most of their thickness

626   below the melting layer (associated with warm processes). However, the Vale do

627   Paraiba rainfall events display a different behavior, in which a very small portion,

628   i.e., less than 5%, of the rainfall is associated with warm clouds. This clearly shows

629   a distinction between coastal and continental rainfall events; a different population

630   of rainfall events from warm clouds was observed. This difference could be reason

631   of cloud process in the clean maritime air near the coast and the more polluted air

632   inland.

633   Another regional comparison was performed to evaluate cloud organization using

634   GOES satellite images. Figure 6c shows the cumulative distribution of the

635   convective cloud fraction (defined as 10.7 μm Brightness Temperature smaller than

636   235 K) as a function of the cloud cluster effective radius (an equivalent area circle;

637   effective radius = $(Area/\pi)^{1/2}$). This convective cloud size distribution only includes

638   clouds with very high cloud tops, i.e., colder than 235 K. Therefore, no warm clouds

639   are included. The calculation was performed using the same procedure as

640   employed by Machado and Rossow (1993) over a region centered on the main site

641   with a radius of 250 km. The regional convective cloud size distributions are very

642   similar. Approximately 80% of the convective cloud fraction is explained by cloud

643   organization with radii smaller than 31 km for all regions. Only slight regional

644   differences are noted for convective cloud organization smaller than 31 km

645   effective radius. Alcantara and Belem have fewer small convective clouds than the

646   others sites. Moreover, Vale do Paraiba exhibits more moderately sized systems

647   (approximately 31 km). However, the largest difference is for convective cloud

648   organization larger than 31 km. Santa Maria has the largest cloud organization,

649   probably due to the more baroclinic instability favoring large MCCs and cold fronts.

650   The CHUVA dataset has just begun to be explored, but some clear regional

651   characteristics can already be described. The warm clouds in Alcantara feature very

652   large droplets (disdrometer measurement) and high liquid water contents

653   (microwave radiometer). Several pixels that were classified as stratiform due to the

654   presence of a bright-band exhibiting large reflectivities and rain rates values. It is

655   possible that the ice aloft, prior to the bright-band formation, is sufficiently

656   vigorous to produce larger rain rates than expected for normal stratiform cloud

657 conditions. The largest CAPE found in Alcantara could explain this strength in the

658 ice production. The highest and most prominent bright-band was observed in

659 Alcantara, which agrees with this notion. Deep convective clouds in Fortaleza

660 display the largest amount of rain water below the melting layer. Costa et al. (2000)

661 showed different DSDs for maritime, coastal, continental and polluted warm clouds

662 in the Fortaleza region. They demonstrated a pronounced increase in

663 concentration and decrease in the maximum droplet diameter as the clouds moved

664 from the ocean to the continent into polluted regions. The high CAPE for these

665 coastal sites helps the development of deep convection. However, these coastal

666 tropical sites have more warm rain clouds and less deep convection than the Vale

667 do Paraiba and Santa Maria locations. Several processes must be considered, such

668 as the small concentration of Cloud Condensation Nuclei (CCN) at the coastal sites.

669 Moreover, the larger trade wind inversion could contribute suppressing deep

670 convection and increase warm cloud formation.

671 The deepest clouds were recorded in Santa Maria, Belem and Vale do Paraiba.

672 These are the regions of very deep clouds, often with cloud tops above 15 km, and

673 organized convection with a more dominant ice phase. Belem presented the most

674 developed glaciated layer (above 7 km), whereas Vale do Paraiba displayed the

675 most developed mixed phase layer, i.e., between the melting layer and 7 km

676 (Calheiros and Machado, 2013).

677

678 **7. Summary.**

679

680   CHUVA provides a comprehensive dataset characterizing the main precipitation

681   regimes in Brazil. The project consistently uses a core complement of

682   instrumentation for each campaign and has recorded and made available high

683   spatial and temporal resolution observations (ground and satellite based) of cloud

684   and precipitation characteristics.

685   CHUVA field campaigns around the tropical region of Brazil provide education and

686   training with respect to the employed instrumentation and the physical processes

687   describing cloud and rainfall formation. CHUVA takes advantage of the

688   instrumentation to present a nowcasting test-bed based on the SOS-CHUVA. The

689   CHUVA data are available through the website, which includes all of the

690   information on each campaign, daily reports, data strategy, quick looks, instrument

691   locations and photos.

692   The CHUVA project contributes to the GLM effort to develop algorithms based on

693   the planned GOES-R and METEOSAT third generation lightning sensors and the

694   preparation of the GPM validation and algorithm development. The large number

695   of warm rain clouds measured in various regions is an important resource for the

696   satellite precipitation algorithms, especially for GPM, to test the ability of retrieving

697   rainfall from non-ice scattering clouds over land.

698   Open access to the database will certainly contribute to improving the knowledge

699   of clouds over tropical regions and advance the description and parameterization

700   of cloud processes.

701

702   **8. Acknowledgement**

9. References

Adams,D.K.,R.Fernandes,E.R.Kursinski,J.Maia,L.Sapucci,L.Machado,I.Vitorello,K.Holub,S.Gutman,NazianoFilizola,R.Bennett,2011:A Dense GNSS Meteorological Network for Observing Deep Convection in the Amazon, Atmospheric Science Letters, DOI:10.1002/asl.312

Bailey, J. C., L. D. Carey, R. J. Blakeslee, S. J. Goodman, R. I. Albrecht, C. A. Morales, and O. Pinto, Jr., 2011: São Paulo Lightning Mapping Array (SP-LMA): Deployment and Plans. Proceedings XIV International Conf. on Atmospheric Electricity, Rio de Janeiro, Brazil.

Battaglia, A., P. Saavedra, C. A. Morales, and C. Simmer, 2011: Understanding 3D effects in polarized observations with the ground-based ADMIRARI radiometer during the CHUVA campaign. J. Geophys. Res.,116,D09204, doi:10.1029/2010JD015335.

Berg, W., T. L'Ecuyer, and C. Kummerow, 2006: Rainfall Climate Regimes: The Relationship of Regional TRMM Rainfall Biases to the Environment. J. Appl. Meteor. Climatol.,45, 434–454.

Cadeddu, M. P., J.C. Liljegren, and D. D. Turner, 2013: The Atmospheric Radiation Measurement (ARM) program network of microwave radiometers: instrumentation, data, and retrievals. Atmos. Meas. Tech. Discuss., 6, 3723-3763, doi:10.5194/amtd-6-3723-2013.

Calheiros, A.J.P. and L.A. T. Machado, 2013: The Cloud and Rain Liquid Water Characteristics of Different Precipitation Regimes in Brazil. Atmos. Res.

Cecchini, M. A., L.A.T. Machado, and P. E. A., 2013: Droplet Size Distributions as a Function of Rainy System Type and Cloud Condensation Nuclei Concentrations. Atmos. Res.

Cecil, D. J. and C. B. Blankenship, 2012: Toward a Global Climatology of Severe Hailstorms as Estimated by Satellite Passive Microwave Imagers. J. Climate, 25, 687–703.

Cohen, J. C. P., M. A. F. da Silva Dias, and C. A. Nobre, 1995: Environmental Conditions Associated with Amazonian Squall Lines: A Case Study. Mon. Wea. Rev., 123, 3163–3174.

Costa A. A., C. J. Oliveira, J. C. P. Oliveira, and A. J. C. Sampaio, 2000: Microphysical observations of warm cumulus clouds in Ceará, Brazil. Atmos. Res., 54, 2–3, 167-199.

Cotton, W.R., 1982 : Modification of precipitation from warm clouds-A review. Bull. Amer. Meteor. Soc., 63, 146-160.

Fabry, Frederic, Isztar Zawadzki, 1995: Long-Term Radar Observations of the Melting Layer of Precipitation and Their Interpretation. J. Atmos. Sci., 52, 838–851.

Garreaud, R. D., 2000: Cold air incursions over subtropical South America: Mean structure and dynamics. Mon. Wea. Rev., 128, 2544–2559.

Garstang, Michael, Harold L. Massie, Jeffrey Halverson, Steven Greco, John Scala, 1994: Amazon Coastal Squall Lines. Part I: Structure and Kinematics. Mon. Wea. Rev., 122, 608–622.

Goodman, S. J., J. Gurka, M. DeMaria, T. Schmit, A. Mostek, G. Jedlovec, C. Siewert, W. Feltz, J. Gerth, R. Brummer, S. Miller, B. Reed, and R. Reynolds, 2012: The GOES-R Proving Ground: Accelerating User Readiness for the Next Generation Geostationary Environmental Satellite System. Bull. Am. Meteor. Soc.,93, 1029-1040. DOI:10.1175/BAMS-D-11-00175.1.

Goodman, S. J., R. J. Blakeslee, W. J. Koshak, D. Mach, J. C. Bailey, L. D. Carey, D. E. Buechler, C. D. Schultz, M. Bateman, E. McCaul, and G. Stano, 2013: The GOES-R Geostationary Lightning Mapper. Atmos. Res., Volumes 125–126, 34-49.

Höller, H., H.-D. Betz, C.A. Morales, R. Blakeslee, J. C. Bailey and R. I. Albrecht, 2013: Multi-sensor field studies of lightning and implications for MTG-LI. 2013 EUMETSAT Meteorological Satellite Conference and 19th American Meteorological Society (AMS) satellite meteorology, oceanography, and climatology conference, September 16-20, Vienna, Austria.

Kouadio Y.K., J. Servain, L. A. T. Machado and C. A. D. Lentini, 2012: Heavy rainfall episodes in the eastern northeast Brazil linked to large-scale ocean-atmosphere conditions in the tropical Atlantic. Advances in Meteorology, 2012, ID 369567, doi 10.1155/2012/369567

Liu, C. and E.J. Zipser, 2009: Warm Rain in the Tropics: Seasonal and Regional Distributions Based on 9 yr of TRMM Data. J. Climate, 22, 767–779.

Liu, Chuntao, Earle R. Williams, Edward J. Zipser, Gary Burns, 2010: Diurnal Variations of Global Thunderstorms and Electrified Shower Clouds and Their Contribution to the Global Electrical Circuit. J. Atmos. Sci., 67, 309–323.

Machado, L. A. T., W. F. S. Lima, O. Pinto Jr, and C. A. Morales, 2009: Relationship between cloud-ground discharge and penetrative clouds: a multi-channel satellite application. Atmos. Res., 93, 304-309.

Machado L. A. T. and W. B. Rossow, 1993: Structural characteristics and radiative properties of tropical cloud clusters. Mon. Wea. Rev., 121, 3234–3260

Morrison, H. and W. W. Grabowski, 2007: Comparison of Bulk and Bin Warm-Rain Microphysics Models Using a Kinematic Framework. J. Atmos. Sci.,64, 2839–2861.

Morales, C.A., L. A. T. Machado, C. F. de Angelis, M. A. F. da Silva Dias, G. Fisch, D. Vila, J. Sakuragi, I. C. Carvalho, J.R. Neves, E.M. Anselmo, and T. Biscaro, 2013: Evaluation of TRMM PR Rainfall Estimates Over Brazil: A Contribution of CHUVA Project. Atmos. Res. (submitted).

Negri, R. G., L. A. T. Machado, S. English and M. Forsythe, 2013: Combining Cloud Resolving Model with Satellite for Cloud Process Model Simulation Validation. J. Appl. Meteor. Clim., in press.

Negri, Andrew J., Emmanouil N. Anagnostou, Robert F. Adler, 2000: A 10-yr Climatology of Amazonian Rainfall Derived from Passive Microwave Satellite Observations. J. Appl. Meteor., 39, 42–56.

Peters, G., B. Fischer, H. Münster, M. Clemens, and A. Wagner, 2005: Profiles of Raindrop Size Distributions as Retrieved by Micro rain Radars. J. Appl. Meteor., 44, 1930-1949.

Rickenbach T.M, 2004: Nocturnal Cloud Systems and the Diurnal Variation of Clouds and Rainfall in Southwestern Amazonia. Mon. Wea. Rev., 132, 1201-1219.

Salio, P., M. Nicolini and E. J. Zipser, 2007: Mesoscale Convective Systems over Southeastern South America and Their Relationship with the South American Low-Level Jet. Mon. Wea. Rev., 135, 1290–1309.

Sapucci, L. F., L. A. T. Machado, J. F. G. Monico, and A. Plana-Fattori, 2007: Intercomparison of Integrated Water Vapor Estimates from Multisensors in the Amazonian Region. J. Atmos. Oceanic Technol.,24, 1880–1894.

Schneebeli, M., J. Sakuragi, T, Biscaro, C. F. de Angelis, I. Carvalho da Costa, C. A. Morales, L. Baldini, and Machado, L. A. T, 2012a.: Observations of tropical rain with a polarimetric X-band radar: first results from the CHUVA campaign, Atmos. Meas. Tech. Discuss., 5, 1717-1761 (.doi:10.5194/amtd-5-1717-2012)

Schneebeli, M., J. Sakuragi, T. Biscaro, C. F. de Angelis, I. Carvalho da Costa, C. A. Morales, L. Baldini, and Machado, L. A. T, 2012b: Polarimetric X-band weather radar measurements in the tropics: radome and rain attenuation correction. Atmos. Meas. Tech.,5, 2183-2199.

Schumacher, Courtney, Robert A. Houze, 2003: Stratiform Rain in the Tropics as Seen by the TRMM Precipitation Radar. J. Climate, 16, 1739–1756.

Silva Dias MAF (Ed.) (2009) As chuvas de novembro de 2008 em Santa Catarina: um estudo de caso visando à melhoria do monitoramento e da previsão de eventos extremos. Nota técnica. São José dos Campos, INPE. 67p.

Schultz, Christopher J., Walter A. Petersen, Lawrence D. Carey, 2009: Preliminary Development and Evaluation of Lightning Jump Algorithms for the Real-Time Detection of Severe Weather. J. Appl. Meteor. Climatol., 48, 2543–2563.

Tapiador, F.J., F.J. Turk, W. Petersen, A. Y. Hou, E. G. Ortega, L. A. T. Machado, C. F. Angelis, P. Salio, C. Kidd, G. J. Huffman, and M. Castro, 2012: Global precipitation measurement: methods, datasets and applications. Atmos. Res.,104–105, 70-97.

Testud, J., E. Le Bouar, E. Obligis and M. Ali-Mehenni, 2000: The rain profiling algorithm applied to polarimetric weather radar, J. Atmos. Oceanic Technol., vol. 17, 322-356.

Tokay, A. and Short, D.A. Evidence from tropical raindrop spectra of the origin of rain from stratiform versus convective clouds. J. Appl. Meteorol., 35, 355-371, 1996

Tokay, A., A. Kruger, and W. Krajewski, A. Perreira, 2002: Measurements of drop size distribution in southwestern Amazon region, J. Geophys. Res., 107 (D20).

Vandenberghe, F., 2003: A multichannel radiometric profiler of temperature, humidity, and cloud liquid. Radio Sci., 38, 8079.

Vila, D. A., L. A. T. Machado, H. Laurent and I. Velasco, 2008: Forecast and Tracking the Evolution of Cloud Clusters (ForTraCC) Using Satellite Infrared Imagery: Methodology and Validation. Wea. Forecasting, 23, 233–245.

Voss, P.B., E.E. Riddle, and M.S. Smith, 2005: Altitude Control of Planetary Balloons. J. of Aircraft, 43, 478-482.

Ware, R., R. Carpenter, J. Güldner, J. Liljegren, T. Nehrkorn, F. Solheim, and F. Vandenberghe (2003). Radio Sci., 38(4), 8079, doi:10.1029/2002RS002856.

Williams, E. R., Stanfill, S. B., The Physical Origin of the Land-Ocean Contrast in Lightning Activity, Comptes Rendus Physique, Volume 3, Number 10, pp. 1277-1292, 2002.

Williams, E., R. Boldi, A. Matlin, M. Weber, S. Hodanish, D. Sharp, S. Goodman, R. Raghavan, and D. Buechler, The behavior of total lightning activity in severe Florida thunderstorms, Atmospheric Research, 51, 245-265, 1999.

Zipser, E. J., C. Liu, D. J. Cecil, S. W. Nesbitt, and D. P. Yorty, 2006: Where are the most intense thunderstorms on earth?.Bull. Amer. Meteor. Soc., 87, 1057–1071.
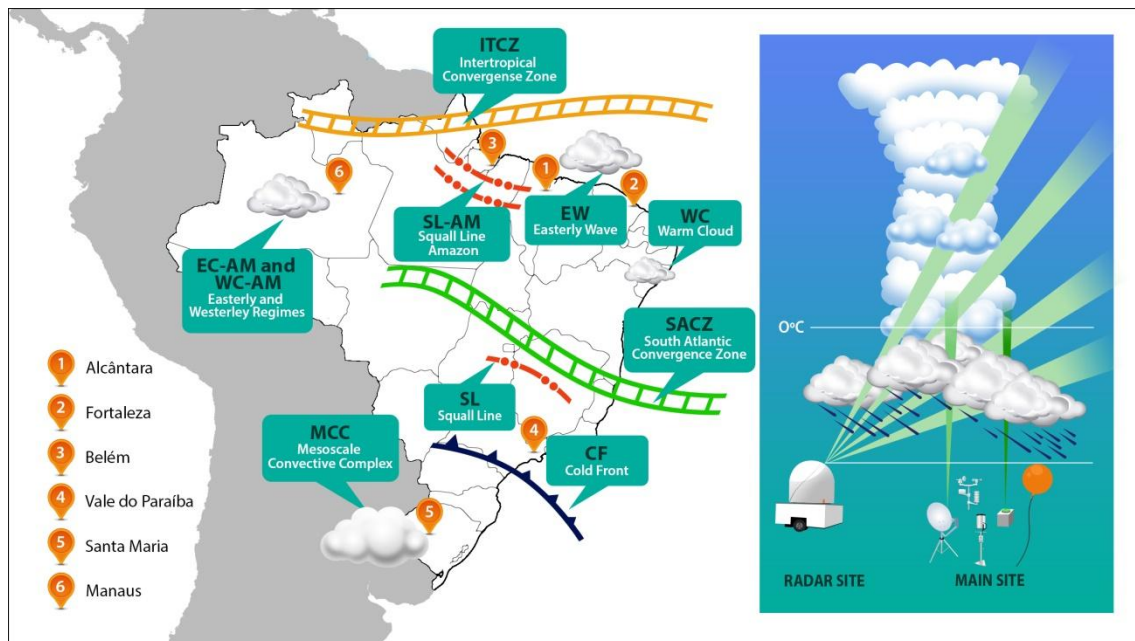
FIGURE CAPTIONS

Figure 1: A description of the CHUVA field campaigns over Brazil and an illustration of the main precipitation regimes. On the right, the diagram describes the reference measurement strategy adopted during the field campaigns, along with the radar site and main site with other ground instruments.

Figure 2: The CHUVA webpage (center) and examples of the data access panel (left) and the web page for the Vale do Paraiba campaign (right). Additionally, one example picture (bottom) showing the radar installation for the Vale do Paraiba campaign is shown.

Figure 3: The sequence of the RHI over a squall line crossing the main site. The illustration is presented for each hour from 17:00 to 24:00 UTC (June 7, 2011) for the Belem field campaign.

Figure 4: The coincident lightning observations on February 10, 2012 at 1900 UTC during a Lightning Imaging Sensor (LIS) overpass from approximately 19:01:10 to 19:03:24 UTC. The plotted ground-based lightning data are limited both temporally and spatially to the LIS overpass limits. The left panel shows the LIS pixels (grey squares) and the ground strikes detected by LMA VHF sources (the colored dots are function of the time). The projections east–west (top) and north-south (left) as functions of the altitude and the number of sources as a function of the altitude are also shown in the left panel.

Figure 5: A) Accumulated LMA lightning source density (number of sources in a 1x1 km grid box during a 15-minute period) for a hail-producing convective cell on 7 January 2012. The upper panels show a plan (latitude-longitude) view and the bottom panels show height-longitude views of the convective cell. Horizontal black lines in the bottom panels indicate the approximate heights of the -10^oC and -40^oC isotherms, where most of the electrical charge transfer occurs. B) Time evolution of the maximum reflectivity and the number of LMA lightning sources. Red lines indicate hail

occurrences in São Paulo and Guarulhos (the two cities showed in panels of A). Only data from the hail-producing convective cell are shown.

Figure 6: A) The DSD gamma parameters for Vale do Paraiba (black dots), Belem (brown dots) and Santa Maria (white dots) in the three-dimensional space composed by N_0, m and Λ. The color of the interpolated surface is associated with the Λ values. B) The cumulative rainfall as a function of the WII (warm cloud–ice cloud index) for Alcantara, Fortaleza, Belem and Vale do Paraiba. LCL stands for lifting condensation level. C) The cumulative convective cloud cover (Tir<235K) as a function of the cloud cluster effective radius for each campaign.

Figure 1: A description of the CHUVA field campaigns over Brazil and an illustration of the main precipitation regimes. On the right, the diagram describes the reference measurement strategy adopted during the field campaigns, along with the radar site and main site with other ground instruments.

Figure 2: The CHUVA webpage (center) and examples of the data access panel (left) and the web page for the Vale do Paraiba campaign (right). Additionally, one example picture (bottom) showing the radar installation for the Vale do Paraiba campaign is shown.

Figure 3: The sequence of the RHI over a squall line crossing the main site. The illustration is presented for each hour from 17:00 to 24:00 UTC (June 7, 2011) for the Belem field campaign.
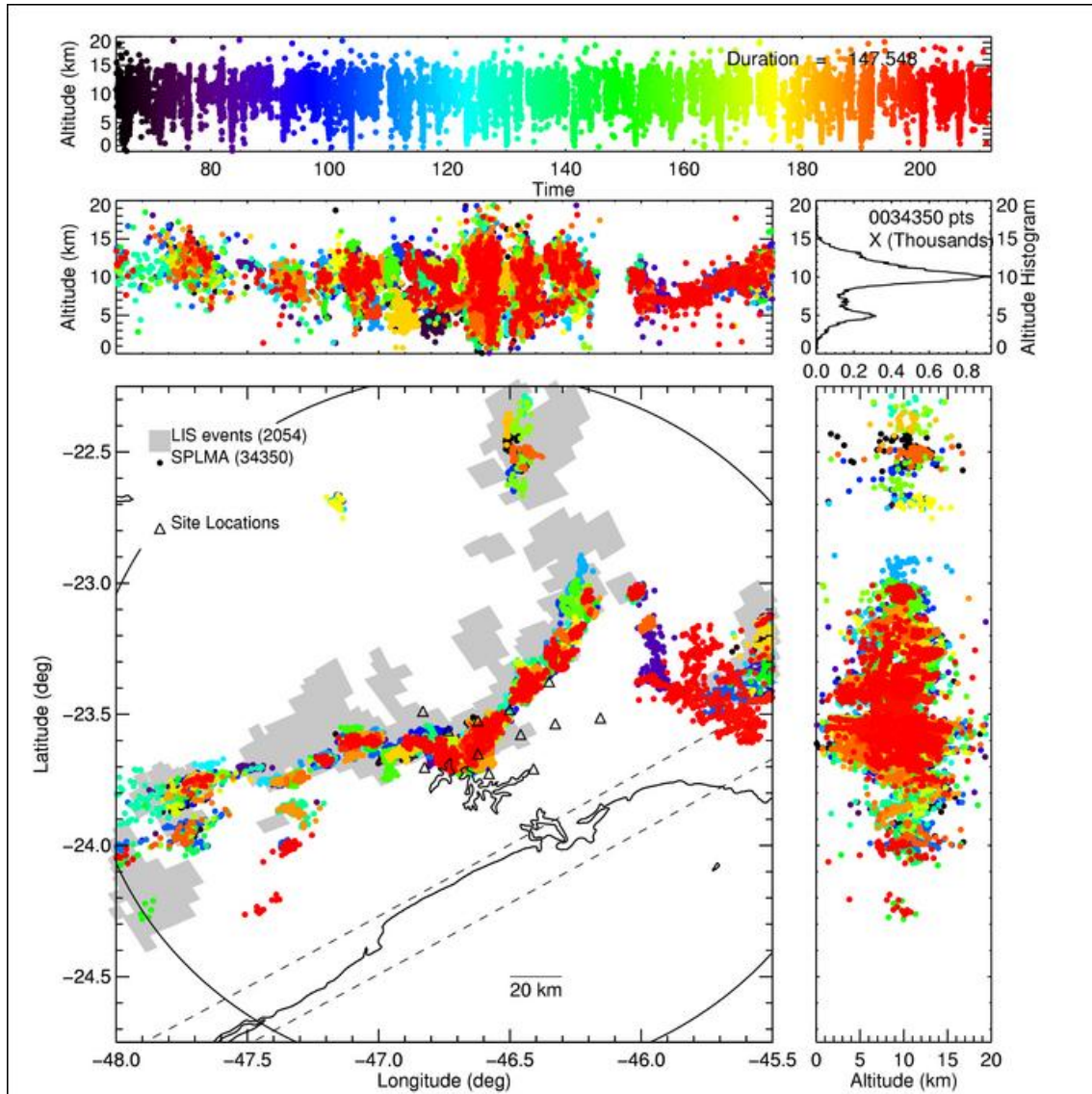
Figure 4: The coincident lightning observations on February 10, 2012 at 1900 UTC during a Lightning Imaging Sensor (LIS) overpass from approximately 19:01:10 to 19:03:24 UTC. The plotted ground-based lightning data are limited both temporally and spatially to the LIS overpass limits. The left panel shows the LIS pixels (grey squares) and the ground strikes detected by LMA VHF sources (the colored dots are function of the time). The projections east–west (top) and north-south (left) as functions of the altitude and the number of sources as a function of the altitude are also shown in the left panel.
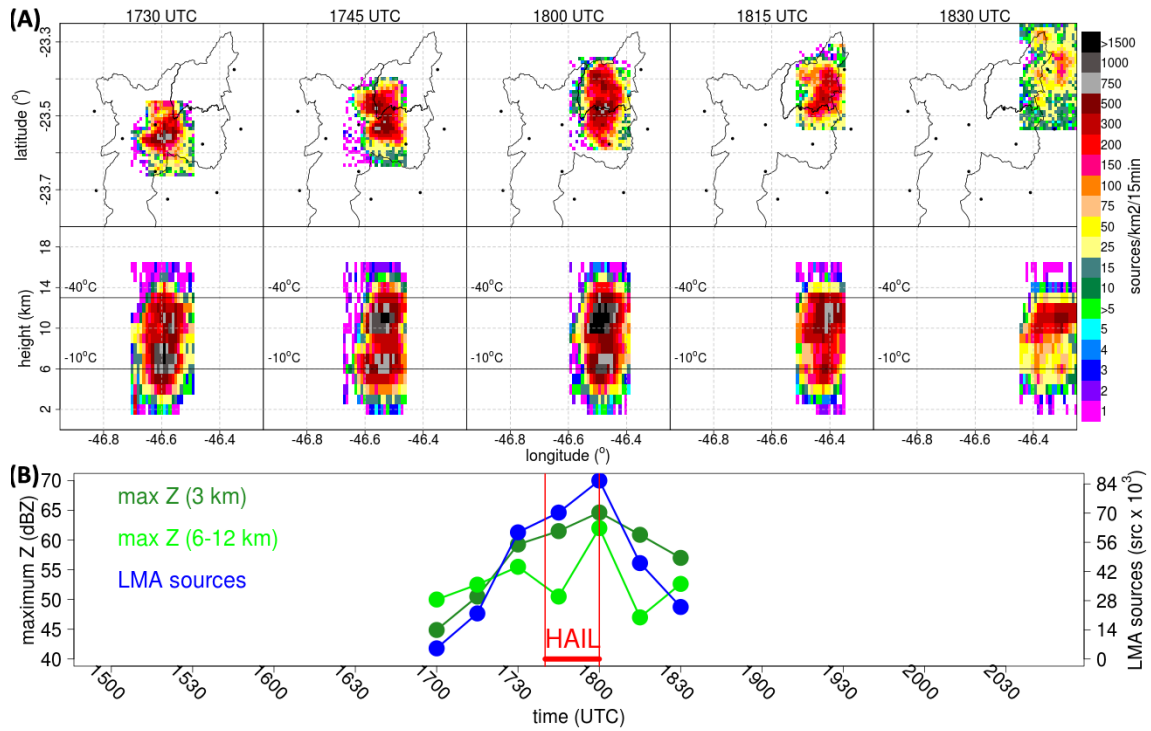
Figure 5: A) Accumulated LMA lightning source density (number of sources in a 1x1 km grid box during a 15-minute period) for a hail-producing convective cell on 7 January 2012. The upper panels show a plan (latitude-longitude) view and the bottom panels show height-longitude views of the convective cell. Horizontal black lines in the bottom panels indicate the approximate heights of the -10°C and -40°C isotherms, where most of the electrical charge transfer occurs. B) Time evolution of the maximum reflectivity and the number of LMA lightning sources. Red lines indicate hail occurrences in São Paulo and Guarulhos (the two cities showed in panels of A). Only data from the hail-producing convective cell are shown.
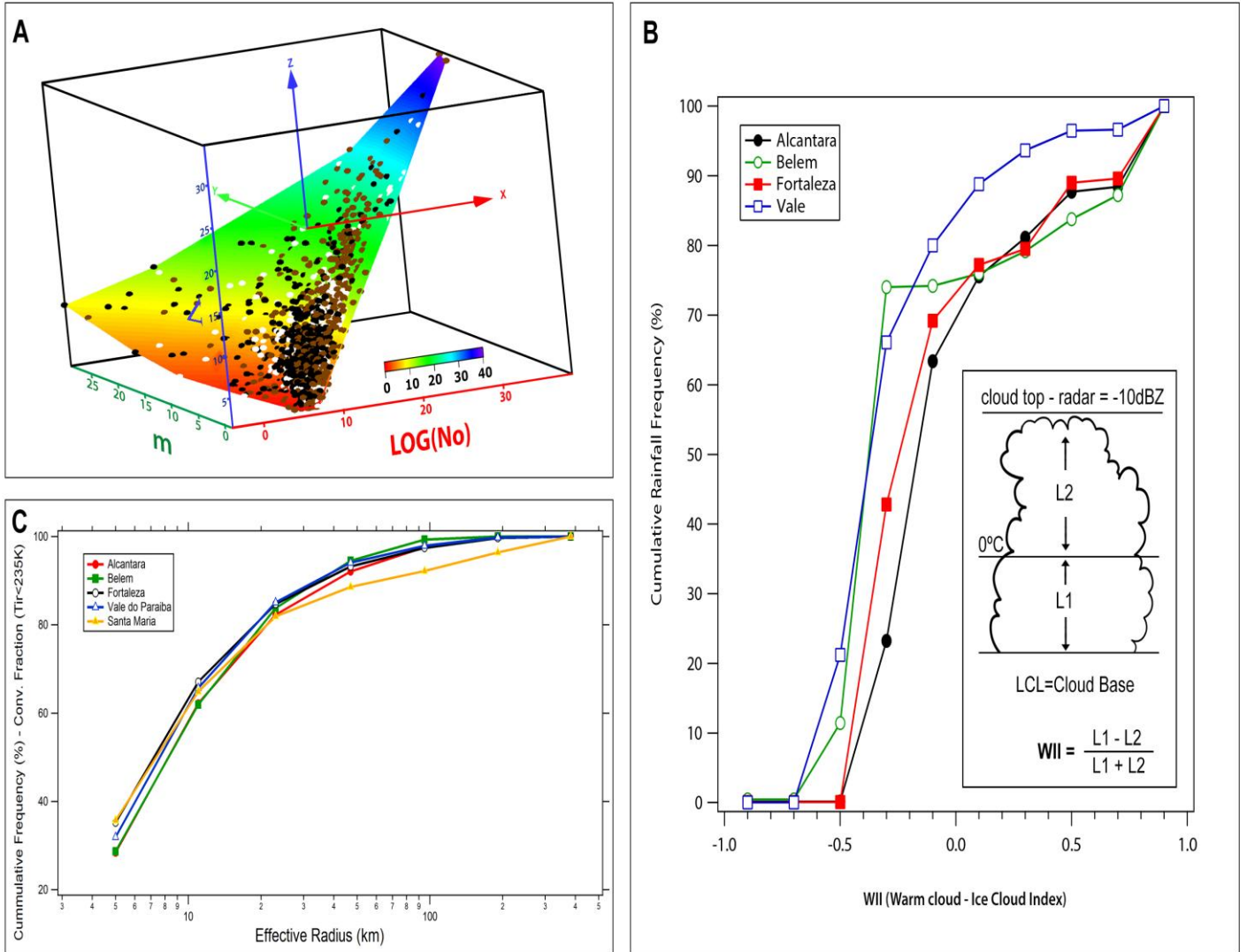
Figure 6: A) The DSD gamma parameters for Vale do Paraiba (black dots), Belem **(brown dots) and Santa Maria (white dots) in the three-dimensional space composed** by N_0, m and Λ. The color of the interpolated surface is associated with the Λ values. B) The cumulative rainfall as a function of the WII (warm cloud–ice cloud index) for Alcantara, Fortaleza, Belem and Vale do Paraiba. LCL stands for lifting condensation level. C) The cumulative convective cloud cover (Tir<235K) as a function of the cloud cluster effective radius for each campaign.

TABLE I: Description of the experiment period, additional instruments and the radars employed during each campaign and a description of the instruments at the main site.

Experiment	Period	Additional Instruments	Radars
Alcantara	2010-03-01 - 2010-03-25	ADIMIRARI Radiometer	EEC X-Band Dual Pol Radar
Fortaleza	2011-04-03 - 2011-04-28		Gematronik Meteor 50DX XPOL Radar
Belem	2011-06-01 - 2011-06-30	Controlled Meteorological balloons and GPS network	Gematronik Meteor 50DX XPOL Radar and S-Band Doppler Radar
Vale do Paraiba	2011-11-01 - 2012-03-31	Lightning detection networks and high-speed cameras.	Gematronik Meteor 50DX XPOL Radar and 2 S-Band Doppler
Santa Maria	2012-11-05 - 2012-12-12	Mesoscale network of automated weather station	IACIT 2 S-Band Doppler Radars
Main Site			
Instruments	Manufacture	Measurement	Retrieval Parameter
Microwave radiometer	MP3000A (Radiometrics)	35 microwave Brigh. Temp. channels (22-30 and 51-58IR infrared channel (9-11μm)	Temperature, Humidity, Water Vapor Density and Liquid Water profiles and integration
Disdrometer	JOSS-WALDVOGEL (RD-80, Disdromet Ltd.) and PARSIVEL (Ott Inc.)	Drop Size Distribution (DSD) Impact (Joss- Valdwogel) and Laser (Parsivel)	DSD, Rain Rate, Liquid Water Content and Terminal Velocity
Rain Gauge	Tipping buck (Hydrological Services Rain Gage 0.01 inch (0.254mm)	Rainfall	Rain Rate
Vertical Pointing Radar	Micro Rain Radar (MRR-2), vertical pointing - 24.1GHz (METEK)	Doppler spectral	Reflectivity, Rain Rate, Liquid Water Content, Terminal Velocity, and Path-Int. Attenuation
LIDAR	Light Detection and Raging - visible Raman Lidar at 532/604 nm (LB10 D-200, Raymetrics)	Backscattering extinction profile	Cloud and aerosol extinction profile, and cloud thickness
GPS	Trimble NetR8 GNSS receptor dual frequency.	Zenithal Tropospheric delay	Integrated Water Vapor
Surface Tower	Solar Kipp & Zonen instruments, Campbell Scientific and Li-Cor, Inc. weather instruments, CS7500, open path analyzer measuring CO_2 and H_2O surface fluxes using eddy cov. tech.	Surface weather variables, soil and temperature, radiative budget and CO_2 and H_2O eddy covariance	Radiative budget, soil temperature and moisture, surface air relative humidity, temperature and wind, moisture, CO_2 and heat fluxes.